Building and Environment 272 (2025) 112664

Contents lists available at ScienceDirect

Building and Environment

journal homepage: www.elsevier.com/locate/buildenv

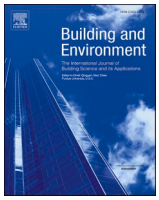

Atmospheric wind effects on depressurization for indoor asbestos pollution containment: Experimental analysis and a ventilation network model validation

A.K.R. Jayakumari [a,b,*], R. Guichard [b], S. Gillmeier [a], A. Ricci [a,c], B. Blocken [d,e]

[a] Building Physics and Services, Department of the Built Environment, Eindhoven University of Technology, Eindhoven, the Netherlands
[b] Department of Process Engineering, Institut National de Recherche et de Sécurité, Nancy, France
[c] Department of Science, Technology and Society, University School for Advanced Studies IUSS Pavia, Pavia, Italy
[d] Institute of Mechanical, Process and Energy Engineering, School of Engineering and Physical Sciences, Heriot-Watt University, Edinburgh, Scotland, United Kingdom
[e] Building Physics and Sustainable Design, Department of Civil Engineering, KU Leuven, Leuven, Belgium

ARTICLE INFO

Keywords:
Hazardous pollution
Atmospheric wind
Air quality
Ventilation network model
Mechanical ventilation
Wind-tunnel testing
Asbestos abatement

ABSTRACT

Hazardous pollutant containment zones in buildings should be depressurized by a dedicated mechanical ventilation system to prevent pollutants from escaping from the indoor to the outdoor atmosphere. Depressurization can be affected by atmospheric wind conditions, which can cause a momentary breach. The goal of this study is to analyze the effect of wind velocity and direction on depressurization and potential containment breaches and to validate a ventilation network model for indoor pressure and breach prediction. Wind-tunnel (WT) tests are performed on a reduced-scale isolated building model equipped with a properly downscaled mechanical ventilation system. The time series of the external pressures (p_e) on the building surfaces and the indoor pressure (p_i) are measured simultaneously. As an alternative approach, a ventilation network model is designed that uses the p_e data from the WT tests to determine p_i. The network model is then validated by comparing the p_i and breach occurrence results by the WT tests versus those by the network model. It is shown that although negative p_i can be maintained continuously, containment breaches occur locally where and when p_e exceeds p_i. The breach probability depends strongly on both wind speed and direction. The network model is successfully validated, where the deviation in breach prediction by the network model is less than 10% compared to the results from WT data alone. The results also show that a -20 Pa depressurization may not be sufficient to avoid a containment breach, which stresses the importance of this and future research on this topic.

1. Introduction

Hazardous pollutants in buildings that threaten public and occupational health should be properly contained through depressurization via dedicated mechanical ventilation system. Asbestos, a fibrous material known for heat resistance, strength, durability, and most importantly abundant availability, has been extensively used in the building sector for decades in the past century [1]. However, studies in the second half of the past century, have revealed that inhaling fibrous asbestos particles could lead to severe health issues, including asbestosis, lung cancer, and mesothelioma of the pleura and peritoneum (e.g., [2–4]). Despite the European Union (EU) implementing a full ban on asbestos use in 2005 [5], it continues to be the leading cause of occupational cancer in the EU. According to the International Commission on Occupational Health (ICOH), asbestos is responsible for an estimated 88,000 deaths annually in Europe, accounting for 55–85% of work-related lung cancer cases [6]. Consequently, caution regarding asbestos-containing buildings became imperative [7].

Asbestos-containing materials in buildings (such as insulation around pipes, ducts, boilers, in ceiling and floor tiles, or as surface materials on walls) may not necessarily generate fibers. However, activities like renovation, demolition or damage to these materials can suspend hazardous fibers with potentially fatal consequences [8–10]. Thus, it is advised to carefully remove asbestos from existing buildings prior to circumstances initiating fiber releases. In Europe, this issue is particularly pressing due to the European Commission's Renovation

* Corresponding author.
E-mail addresses: a.k.radhakrishnan.jayakumari@tue.nl (A.K.R. Jayakumari), romain.guichard@inrs.fr (R. Guichard), s.g.gillmeier@tue.nl (S. Gillmeier), a.ricci@tue.nl (A. Ricci), b.blocken@hw.ac.uk (B. Blocken).

https://doi.org/10.1016/j.buildenv.2025.112664
Received 3 November 2024; Received in revised form 14 January 2025; Accepted 2 February 2025
Available online 3 February 2025

Wave, which aims to renovate 35 million buildings by 2030 to enhance energy efficiency. Approximately 85% of EU buildings are constructed before 2001, a time when asbestos was commonly used, and nearly 75% are considered energy inefficient by today's standards [11]. As a result, asbestos removal has become a significant challenge for the construction industry and public health.

The asbestos removal process involves the suspension of hazardous fibers in dangerous concentrations and should therefore be performed under controlled conditions. This requires sealing the containment and establishing a negative pressure inside with respect to the outdoor environment (e.g., [12–15]). This is achieved through the implementation of a properly designed mechanical ventilation system equipped with a negative pressure unit including a high-efficiency particulate air (HEPA) filter [12]. The outflow from the containment passes through the HEPA filter that removes the hazardous particle from the exhaust air. In addition, the laborers working inside the enclosure use effective respiratory protective equipment (PPE) and coveralls to protect themselves from asbestos exposure.

Regulatory authorities in different countries have established guidelines for the asbestos abatement processes (e.g., [13],[16–19]) which include specific requirements for depressurization and air change per hour. To prevent asbestos fiber leakage, depressurization of -5 Pa to -40 Pa relative to the outdoor environment is recommended. While some research publications (e.g., [20],[21]) examined the adequacy of existing guidelines for situations such as entry and exit of workers, changes in the negative pressure unit (NPU) airflow because of filter clogging, the relative positioning of ventilation components, the influence of atmospheric wind conditions on this depressurization has not yet been adequately studied.

When wind interacts with a building, it creates high negative pressure on parts of the facade. If this negative surface pressure exceeds the internal pressure induced by the mechanical ventilation, breach can occur, allowing asbestos fibers to escape to the outdoor environment through leaks. Field measurements performed in a high-rise building by Papadopoulos et al. [22] revealed that a breach in asbestos containment is possible because of wind effects. This poses significant health risks to both on-site laborers and the public in the vicinity. In particular, the involved laborers have risks associated with long-term exposure as they do not generally wear the respiratory protection equipment (RPE) while outside the enclosure. Thus, understanding the impact of wind on depressurization in asbestos containment zones is critical for occupational and public health.

Atmospheric boundary layer wind tunnels (ABLWT) have been used extensively for studying wind-structure interactions (e.g., [23–28]). ABLWTs allow tests to be conducted under controlled conditions to study the influence of individual parameters such as wind speed and direction. WTs have been extensively used for studies involving naturally ventilated buildings (e.g., [29–38]) and mechanically ventilated buildings (e.g., [39–42]). These studies showed that external wind conditions have a significant influence on the airflow conditions within a ventilated building. In particular, the studies of Etheridge [30] and Wang et al. [32] revealed the possibility of undesirable flow reversal because of the effect of instantaneous wind pressures. The WT tests performed on mechanically ventilated buildings by Le Roux et al. ([39], [40]) and Le Dez et al. [41] also showed the possibility of breach in mechanically depressurized buildings in nuclear facilities due to atmospheric wind effects. However, the findings from nuclear facilities cannot be directly applied to asbestos removal, as the two contexts differ significantly. These differences include the type of containment—permanent in the nuclear industry and temporary in asbestos abatement—as well as leakage rates, layouts of depressurized compartments, materials, ventilation duct lengths, fan characteristics, air change rates, targeted negative pressures, usage durations, and associated exposure risks. This underscores the need for new, sector-specific knowledge tailored to the asbestos removal industry.

The goal of the present study is twofold: (1) to analyze the effect of wind velocity and direction on depressurization and potential containment breaches; and (2) to validate a ventilation network model to predict indoor pressure and breach occurrence.

In the first part of this study, WT tests are performed for a reduced-scale isolated building model equipped with a properly downscaled mechanical ventilation system. The scaling of this system is executed by following the methodology proposed by Le Roux et al. [39]. This methodology was previously validated for usability in a depressurized nuclear power plant and later fine-tuned by Jayakumari et al. [43] for WT testing. In the present study, time series of the external pressures (p_e) on the building surfaces and the indoor pressure (p_i) are measured simultaneously during the WT tests for multiple wind speeds and directions. This enables a systematic analysis of the effects of wind speed and direction on internal depressurization for asbestos containment, as well as on potential breaches during the abatement process.

The second part of this study aims at evaluating the reliability of the ventilation network model SYLVIA [44] for predicting the internal pressure and potential containment breaches. The p_e obtained from the WT tests are used as input for the network model to predict p_i in the containment zone and the potential occurrence of breaches. The results of the network model are then validated with the p_i measured during the WT tests. The ventilation network model SYLVIA is adopted in this study because it has already been validated for applicability in nuclear power plants where, similar to asbestos abatement plants, a depressurization is established with respect to the outdoor environment ([40],[41]).

The paper is structured as follows: Section 2 provides a detailed description of the WT setup and ABL wind characteristics. It introduces the case study building equipped with the scaled mechanical ventilation system for the asbestos abatement process and it outlines the scaling methodology used for testing at reduced scale. This section also provides an overview of the ventilation network model. Section 3 presents the WT results and the validation of the network model. Section 4 discusses the relevance of findings to a real asbestos abatement process. Section 5 summarizes and concludes the paper.

2. Methodology

The flow chart in Fig. 1 shows the outline of the methodology adopted, which is further elaborated in the subsequent Sections 2.1–2.3.

2.1. Building and ventilation system

For this study, a containment volume is installed at the upper half of the idealized cubical building model of full-scale dimensions 18 × 18 × 18 m^3. The ventilation system for the containment volume of 18 × 18 × 9 m^3 is designed to maintain a depressurization of -20 Pa and an air change rate of 6 h^{-1} (all full-scale values). The ventilation system is designed following the industry guidelines of [14] and is elaborated in the publication by Jayakumari et al. [43]. The designed ventilation system comprises forty air inlets with check valves (*A1 – A40*), four NPUs (*N1 – N4*), an air inlet for tuning together with an airlock for materials, and an airlock for people. Table 1 shows the dimensions and the operation values of these ventilation components at full scale. Fig. 2a illustrates the building with the ventilation components and Fig. 2b shows the building and its ventilation components on the WT turntable. To account for the building's airtightness, sixteen leakage locations (*L1–L16*) distributed across four facades are included in addition to the ventilation components. These leaks represent unintended openings in the building envelope [52], which may arise from factors such as permeable building materials, expansion joints, or the installation of doors, windows, and mechanical ventilation systems. Such openings are a reality and must be considered in the experiment to account for potential airflow through them. As outlined in Jayakumari et al. [43], this study assumes a leakage rate of 0.15 vol per hour, corresponding to Type I leakage as defined by Dubernet et al. [14]. Leakage types (I–IV) are categorized based on the presence of structural leaks and the level of

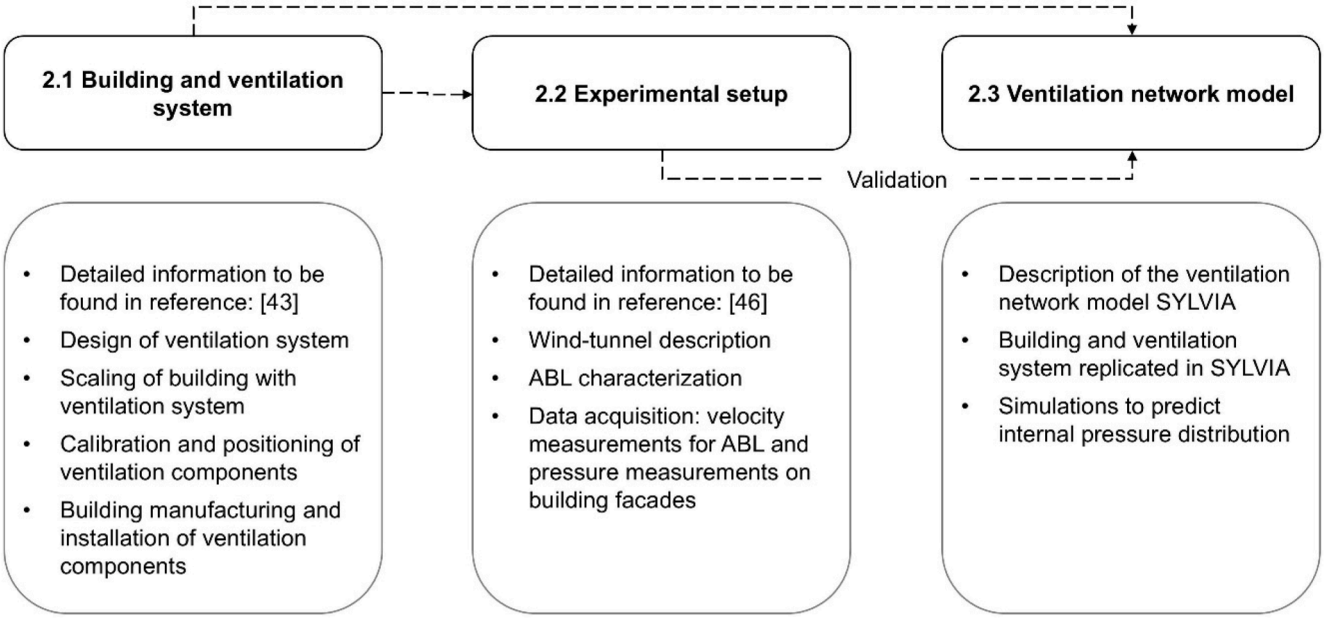

Fig. 1. The outline of the methodology adopted for conducting the study.

Table 1
Operational values and dimensions of the ventilation components.

Ventilation component	Volumetric flow rate (Q) m^3/h	Pressure loss (dP) Pa	Opening area (S) m^2	Length (L) m
NPU	4500	550	0.37	1.0
Air inlet with check valve	410	20	0.03	0.4
Air inlet for tuning	410	20	0.03	0.4
Airlock for material	500	20	0.36	2.0
Airlock for people	400	20	0.36	5.0

confinement achievable through the building envelope. Type I reflects a scenario with no structural leaks and effective envelope confinement, while Type IV represents the worst-case scenario. For more information, readers are advised to refer to Dubernet et al. [14].

2.1.1. Scaling method

The scaling method by Le Roux et al. [39] is adopted for the building and ventilation system. The procedure is briefly discussed in this subsection and detailed further by Jayakumari et al. [43]. The building equipped with the mechanical ventilation system is conceptualized as a network of interconnected "nodes" and "branches". Nodes represent rooms, junctions, or an exterior environment (boundary condition) where properties like pressure, temperature, and pollutant concentration are assumed to be uniform. Branches represent components of the ventilation system, such as air inlets, airlocks, leaks, filters, and fans in the case of asbestos abatement worksites. By applying the mass balance equation to the nodes and the generalized Bernoulli equation to the branches, two dimensionless numbers N_1 and N_2 can be derived as in Eqs. 1.1 and 1.2:

$$N_1 = \frac{R_{ref} S_{ref}^n}{\left(\rho_{ref} U_{ref}\right)^{2-n}} \tag{1.1}$$

$$N_2 = \frac{P_{atm}}{\rho_{ref}} \frac{S_{ref} L_{ref}}{V_{ref} U_{ref}^2} \tag{1.2}$$

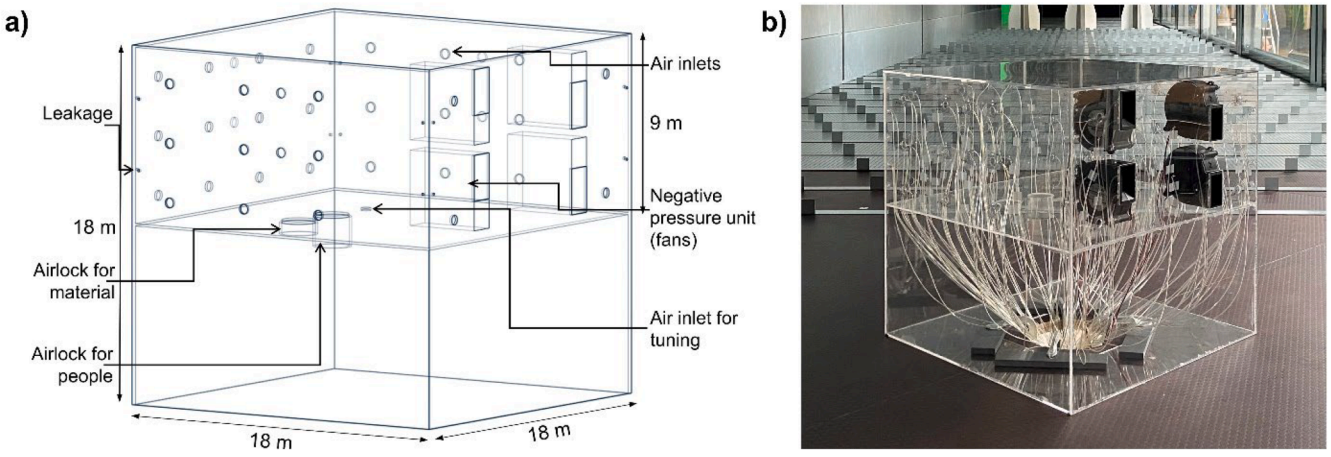

Fig. 2. (a) Schematic diagram of building model with ventilation components; (b) close-up view of reduced-scale building model equipped with properly downscaled mechanical ventilation system and pressure tubes for measurements in the WT.

where R_{ref}, S_{ref}, U_{ref}, ρ_{ref}, L_{ref}, V_{ref} and P_{atm} are the reference values of airflow resistance ($kg^{2-n}/m^4/s^{2-n}$), branch section area (m^2), velocity (m/s), air density (kg/m^3), branch length (m), the volume of the node (m^3) and the atmospheric pressure (Pa), respectively. The exponent "n" depends on the branch type and is equal to 2 for ducts (i.e., for airlocks and air inlets), 1 for NPUs with HEPA filter and between 1 and 2 for leaks. The equality of these numbers (N_1 and N_2) between the full-scale building and the reduced-scale model ensures the necessary geometric, kinematic and dynamic similarity. Additionally, the relationship between different scaling factors is established, namely the velocity scale ($\overline{U}$), pressure scale ($\overline{P}$), volumetric flow rate scale ($\overline{Q}$), time scale ($\overline{t}$), frequency scale ($\overline{f}$), volume scale for the building ($\overline{V}$), length scale for the ventilation openings ($\overline{L}$), and section area scale for the ventilation openings ($\overline{S}$). The volume scale ($\overline{V} = 1{:}40^3$) for the building is predetermined to ensure realistic lengths for the smallest ventilation component that can be feasibly manufactured and physically implemented in the reduced-scale building model, while also adhering to the blockage ratio requirements (i.e., less than 5%) for the WT tests. $\overline{P}$ and $\overline{Q}$ are fixed as 2 and 1:180, respectively, in consideration of the availability of a compact fan that represents the NPU with a HEPA filter. All other scaling factors are defined according to these three fixed scaling factors, as outlined in Table 2.

2.1.2. Building and ventilation system in reduced scale

The building model is manufactured using polymethyl methacrylate (PMMA) with a thickness of 0.003 m (at reduced scale). Air inlets are represented by openings with a diameter of 0.012 m (at reduced scale) in the facades of the building model. The airlock for people and the airlock for materials have a diameter of 0.042 m and are incorporated in the building model using tubes of 0.040 m and 0.016 m length, respectively. Airlocks are assumed to be not exposed to wind and therefore are installed on the floor of the containment volume inside the building, as shown in Fig. 2a. All the ventilation components are calibrated to confirm that they operate at the required reduced-scale volumetric flow rate (Q) versus static pressure loss (dP) characteristics as explained in Jayakumari et al. [43]. The function of the NPU is replicated by four compact fans (dimensions: $97 \times 95 \times 33\ mm^3$) of high pressure-loss (dP) to a low volumetric flow rate (Q) installed within the containment volume. The fans are chosen in such a way that they respect the operating point (i.e., Q versus dP) of the NPU at the reduced scale at a specific supplied voltage. They are set to operate at 25 m^3/h and 1100 Pa with a supply voltage of 12 V, resulting in full-scale Q and dP values for the NPU with HEPA filter of 4500 m^3/h and 550 Pa, respectively. The fans are connected to a power supply positioned below the WT floor so that they can be turned ON/OFF as required for the tests. Leakages are reproduced in the building model by sixteen openings on the facades of 0.003 m in diameter (reduced-scale). The leakage openings are also calibrated to check the adherence to the recommended flow exponent $1/n$ (e.g., [53],[54]), ensuring that real leakages are accurately replicated. In line with the recommendation provided by ASHRAE [53] for which $0.6 \leq n \leq 0.7$, the present study adopts a flow exponent (n) equal to 0.6. Fig. 2b shows a close-up view of the building model installed with all ventilation components and instrumented for external and internal pressure measurements in the WT.

Table 2
Scaling factors to design the reduced-scale building with a mechanical ventilation system.

Parameter	Scaling factor	Parameter	Scaling factor
$\overline{U}$	$\sqrt{2}$	$\overline{V}$	$1{:}40^3$
$\overline{P}$	2	$\overline{L}$	1:126
$\overline{Q}$	1:180	$\overline{S}$	1:225
$\overline{T}$	1:178	$\overline{f}$	178

2.2. Experimental tests

2.2.1. Wind-tunnel setup

The experiments are conducted at the ABLWT facility of Eindhoven University of Technology (TU/e) in the Netherlands (Fig. 3). Building model and ABL flow characteristics are geometrically scaled with a ratio of 1:40. The ABL corresponds to a wind over moderately rough terrain (discussed in Section 2.2.2) and is generated inside the facility by vortex generators and arrays of roughness elements. The former consists of three spires based on the design suggested by Irwin [45] with a base width of 0.5 m and a top width of 0.04 m, along with a base extension. The latter consists of a large number of 'L-shaped' metal elements of size $0.06 \times 0.06\ m^2$ and $0.04 \times 0.04\ m^2$. For more details of the WT setup, readers are directed to Jayakumari et al. [46]. This publication investigated the feasibility of employing a relatively large geometrical scaling ratio for external pressure measurements on a cubical building in ABLWTs of typical cross-section dimensions of 3 (width) $\times$ 2 (height) m^2 and discussed possible implications.

For the present investigation, building model is positioned at the center of a turntable and is equipped with a mechanical ventilation system. The blockage ratio for all tests was below 5%. Tests are conducted for eight wind directions (i.e., $\theta = 0°$, 45°, 90°, 135°, 180°, 225°, 270°, and 315°) where 0°, 90°, 180° and 270° are perpendicular to the building facades. The turntable rotation has an accuracy of ±1°. It is noted that although cubically shaped, the building model is not symmetric because of a non-symmetric arrangement of mechanical ventilation components on the building's façades (presented in Section 2.1 and Fig. 5). Three reference wind speeds (i.e., $U_{ref} = 4.4$, 6.5, 8.5 m/s) corresponding to the streamwise mean velocity component of the approaching flow at building height (H) are tested. Velocities and pressures are presented in full scale throughout the paper, after applying the relevant scaling factors discussed in Sections 2.1.

2.2.2. ABL wind characterization

The characteristics of the ABL wind are measured at the center of the turntable, at the position where the building will be positioned. These are termed incident flow profiles and can be considerably different from the upstream approach-flow profiles, especially near the WT floor ([47], [48]). The streamwise (u), lateral (v), and vertical (w) components of the instantaneous velocity are measured at multiple heights at the center of the turntable. A Series 100 Cobra Probe [49] with an accuracy of ±0.5 m/s is used to record the velocities for a duration of 60 s at 1000 Hz sampling frequency. A fully automated traverse system enabled Cobra probe movement with an accuracy of less than 1 mm. The mean streamwise velocity (U) and turbulence intensity (I_u) profiles are presented in Fig. 4(a,b). The error bars indicate the experimental uncertainties related to U and I_u, calculated using the standard deviation of repeated measurements at building height. The power law and logarithmic law fit for U are also shown. The power law fit yields a power law exponent (α) of 0.17, while the logarithmic law fit provides an aerodynamic roughness length (z_0) of 0.014 m in full scale. This z_0 value represents mean flow characteristics over moderately rough terrain according to VDI-3783 [50]. Fig. 4b also shows that the I_u characteristics fall within the moderately rough terrain classification, with a value of 16% at building height ($H = 18$ m). Fig. 4c shows the normalized power spectral density (S_{uu}) at building height compared to the analytical model by Simiu and Scanlan [51]. It can be observed that the low-frequency range of the spectrum, representing the larger turbulent structures, is not well reproduced. However, for all turbulent structures smaller than the most energetic ones (peak of the normalized power spectral density), the spectrum of the ABL developed in the WT matches relatively well with the analytical model. Thus, the energy cascade in the inertial sub-range and generally the most energetic, turbulent structures as well as the smaller structures are well reproduced (Fig. 2c). The deficiency related to the low-frequency range of S_{uu} typically arises when using relatively large geometric scaling ratios (e.g., 1:40) to

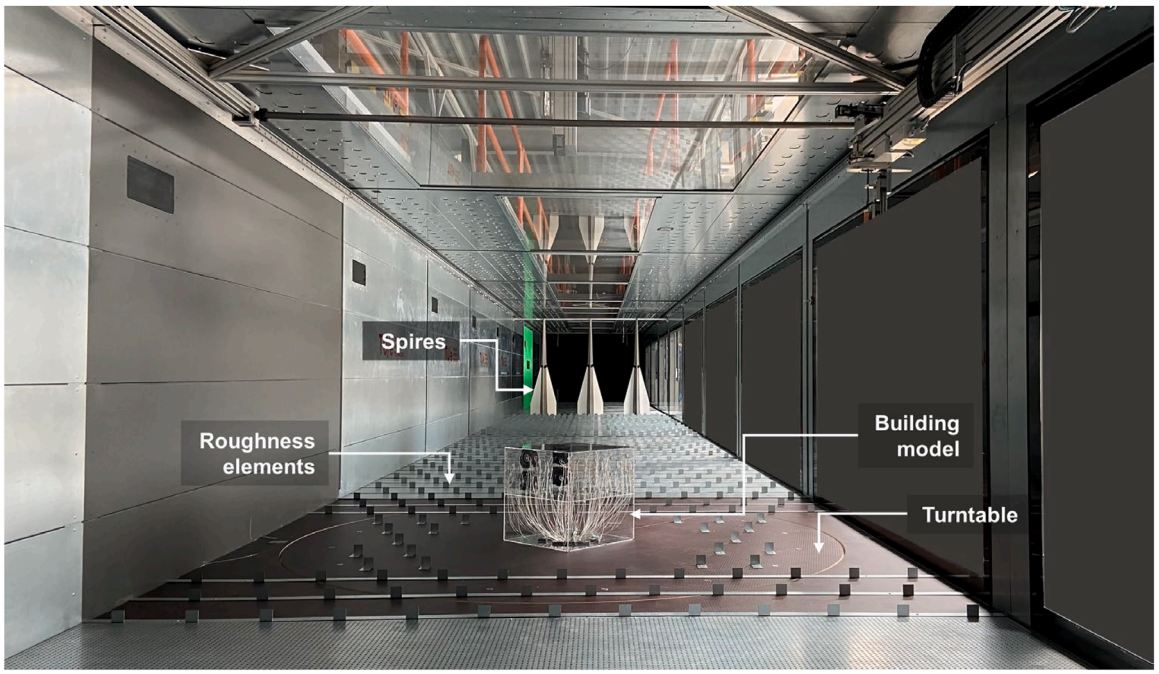

Fig. 3. Photograph of the WT setup with vortex generators (i.e., spires), roughness fetch (i.e., L-shaped metal elements) and building model mounted on the turntable.

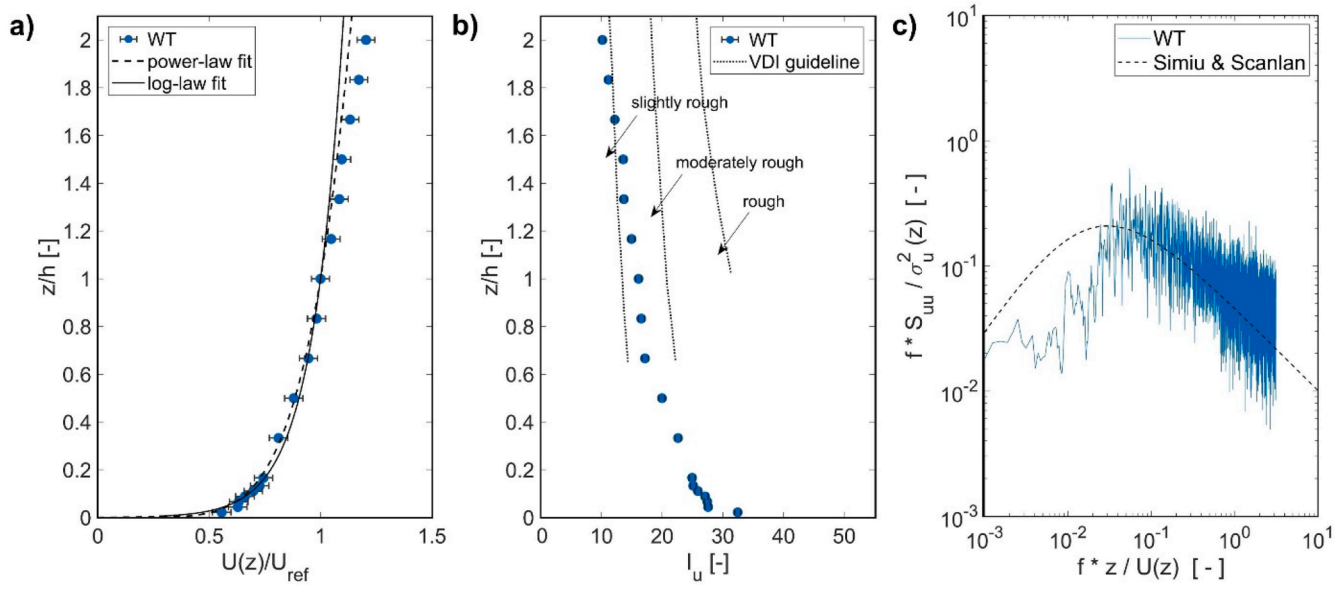

Fig. 4. Incident vertical profiles of (a) streamwise mean wind velocity (U) with logarithmic law and power law fit; (b) streamwise turbulence intensity (I_u) with terrain classification; (c) normalized power spectral density (S_{uu}) at building height with indication of Simiu and Scanlan model [51].

generate ABLs in WTs of typical cross-section dimension (e.g., width × height = 3 × 2 m^2). This limitation may have possible implications when analyzing wind effects on mechanically depressurized containment zones. These were investigated by Jayakumari et al. [46], who focused on a building model with same dimension (18 × 18 × 18 m^3) tested in the WT at geometrical scaling ratios of 1:40 and at 1:300. It was found that using a 1:40 scaling ratio can affect the breach prediction particularly in case the roof is equipped with ventilation components. The study concluded that larger geometrical scaling ratios (such as 1:40) should only be used for mechanical ventilation studies in ABL flows if the roof does not have ventilation components. Furthermore, it is found that results from those tests should be treated with caution because at regions of flow reattachment and recirculation, the probability of a containment breach could be underpredicted by 10%. However, it is crucial to note that the 10% encompass also the combined effects of limitations in building manufacturing, variations in incident flow characteristics (i.e., differences in ABL height and turbulence characteristics), inequality of Jensen numbers between the two scaling cases, in addition to the absence of large-scale structures. Despite these limitations, choosing a relatively larger geometric scaling ratio is inevitable for experimental tests including reduced-scale mechanical ventilation components and the instrumentation for internal/external pressure measurements into the building model. Thus, considering all these aspects, a geometric scaling ratio of 1:40 is chosen for this study and the roof of the cubical

building model is not equipped with ventilation components.

2.2.3. Experimental data acquisition

Fig. 5 shows the location of each ventilation component and each leakage opening on the external facade of the building. Pressure sensors are strategically placed in proximity to each component and leakage openings on the external facade. Additionally, 26 internal pressure sensors are installed at the interior walls and floor of the containment volume. Two Scanivalve MPS4264 pressure scanners [55], each equipped with 64 transducers, are used for the simultaneous recording of p_e and p_i. The sampling duration for each recording session is set to 180 s with a frequency of data acquisition of 800 Hz. The transducers are connected to the pressure sensors on the building surfaces by means of a 1.10 m long urethane tubing with an internal diameter of 1.37 mm. To account for any phase and amplitude distortion caused by the pressure tubing system, tubing transfer functions are used according to the methodology proposed by Irwin et al. [56] for corrections on the pressure time series. The instrument has an accuracy of ±0.20 % of the measurement range, equivalent to ±2 Pa. Repeatability measurements are also conducted for the pressure measurements to ensure reliability of the results. The average deviation in terms of instantaneous peaks is found to be within ±4 Pa for p_e and within ±2 Pa for p_i. The results are presented at full scale in terms of instantaneous pressures p_e, p_i, and differential pressure (Δp) defined as the following Eq. 2:

$$\Delta p = p_i - p_e \tag{2}$$

The mean external pressure coefficient ($C_{pe,mean}$) is defined as the following Eq. 3:

$$C_{pe,mean} = \frac{1}{N_p}\sum \frac{p_e - p_0}{\frac{1}{2}\rho U_{ref}^2} \tag{3}$$

where N_p is the number of pressure samples, p_0 is the reference static pressure outside the building and ρ is the air density.

While measuring p_e and p_i with the fans of the ventilation system ON, some noise caused by the rotation of the same fans has been detected. To remove the harmonic components associated with specific frequencies of this noise (in the range 216 - 222 Hz), a filtering process is applied to all pressure signals.

2.3. The ventilation network model

A numerical simulation of the scenario tested in the WT is conducted with the ventilation network model SYLVIA developed by Institut de Radioprotection et de Sûreté Nucléaire (IRSN) [44]. The SYLVIA version 11.5 is used in this study. This model employs high-resolution time series of external pressure (p_e) as input data, thereby taking into account atmospheric turbulence effects to predict the time series of the internal pressure (p_i) within the containment volume. The input p_e also incorporates the effects of building geometry and the orientation of the building relative to the approach flow. An important advantage of network models lies in their capacity to deliver rapid simulations with low computational resource demands, distinguishing it from other numerical methods, such as computational fluid dynamics (CFD) (e.g., [31],[57]). SYLVIA's user-friendly interface facilitates data import/export and incorporates validation checks, thus reducing the potential for setup errors by users and enabling the design and simulation of complex systems. However, it should be noted that (like other numerical models) network models rely heavily on precise input data (particularly p_e) for accurate predictions of p_i. A limitation of network models is their inability to provide detailed information about the indoor 3D flow field and visualization of indoor airflow patterns. However, for the purpose of this study, predicting the 3D flow field and visualizing airflow patterns is not required.

The network model is a zonal model that conceptualizes the network of buildings and the ventilation system as interconnected nodes and branches. In this context, the nodes represent the containment volume, the junction between branches, and exterior environment (boundary condition), where properties like pressure, temperature, and pollutant

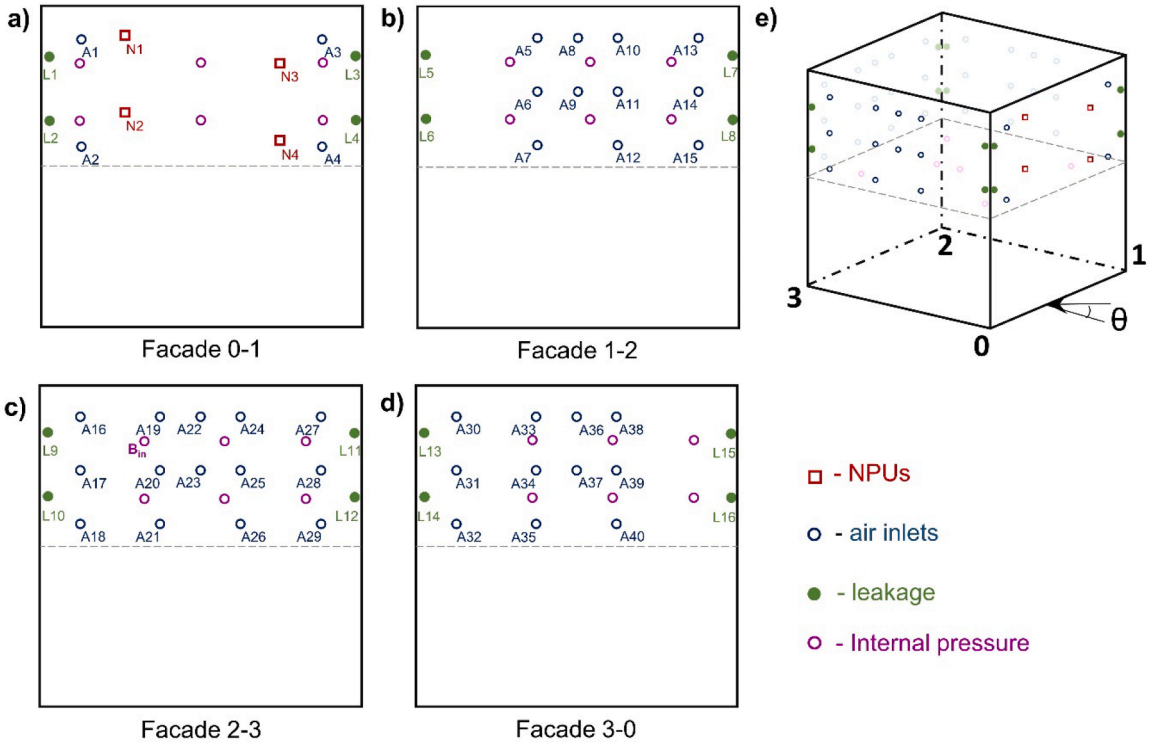

Fig. 5. Location of ventilation components and leakages at building model facades where external pressure time series are recorded. In addition, the locations of internal pressure measurement positions are shown: (a) facade 0–1, (b) facade 1–2, (c) facade 2–3, (d) facade 3–0, and (e) isometric view of the building model.

concentration are assumed to be uniform. The nodes adhere to principles of mass, momentum, and energy conservation, and the following mass balance equation (Eq. 4) ([39],[44]) is used for ventilation studies:

$$\frac{VM}{rT}\frac{dP}{dt} = \sum \rho_i Q_i - \sum \rho_j Q_j \tag{4}$$

where V is the volume of the node, M is the molecular mass of air (28.96 g/mol), T is the ambient temperature, r is the perfect gas constant (8.314 J/mol/K), i and j are subscripts for inlet and outlet flows, respectively. The branches symbolize the various components of the ventilation system, such as air inlets, airlocks, leaks, filters, and fans in the case of asbestos abatement sites. The branches are assumed to be horizontally positioned and the flow isothermal, incompressible and one-dimensional. The calculation of the mass flow rate between nodes is accomplished through the generalized form of the Bernoulli equation for the branches expressed in Eq. 5 ([39],[44]):

$$\frac{\rho L}{S}\frac{dQ}{dt} = \Delta P - \ sgn(Q)R^n\frac{|Q|^n}{\rho^{n-1}} \tag{5}$$

where L is the branch length, S is the branch section area, R is the airflow resistance, and ΔP is the static pressure difference.

The mechanical ventilation system along with the containment volume is replicated in the network model, as illustrated in Fig. 6. *A1 - A40* represent the air inlets with check valves, *N1 - N4* represent the NPUs, *AT1 - AT2* represent the air inlets for tuning, and *AL1* and *AL2* represent the airlock for materials and people, respectively. *L1 - L16* represent the sixteen leakage points that account for the building's airtightness. In the initial stage, the properties of the fluid, the characteristics of the containment volume (depressurization of -20 Pa and the volume of the containment in m^3) as well as the details of each ventilation component (Q versus P characteristics and L and S) are defined in the network model. These inputs are used then to calculate the aeraulic characteristics of each ventilation component by means of Eq. 6 [44] and to establish the initial baseline condition with no external wind effects:

$$\Delta P = R\frac{Q^n}{\rho} \tag{6}$$

where R is the airflow resistance of the corresponding ventilation component.

In the subsequent stage, the p_e time series recorded in the WT at the location of each ventilation component exposed to wind (NPUs and air inlets) as well as leakage locations are provided as input to the network model. The p_i is then calculated for each time-step (i.e., 1.25×10^{-3} s, corresponding to 800 Hz) for a duration of 30 s to predict the temporal change in p_i resulting from the influence of external wind conditions on the flow through the ventilation components. This is done by iteratively solving the ordinary differential Eqs. 4 and 5 for each time step by means of a Newton-Raphson algorithm. Time discretization is performed by means of a backward differential formula, which is particularly effective for stiff equations [58]. Network model simulations are performed for $\theta = 0^\circ$ and $\theta = 45^\circ$ and the results are discussed in Section 3.3.

3. Results

3.1. Scenario 1: mechanical ventilation ON–wind OFF

This subsection presents the p_i generated within the containment zone by the active mechanical ventilation system (mechanical ventilation ON) in the absence of external wind conditions (wind OFF). Fig. 7 displays the time series of p_i obtained from all 26 internal pressure sensors for this scenario. A representative segment of 0.2 s from the

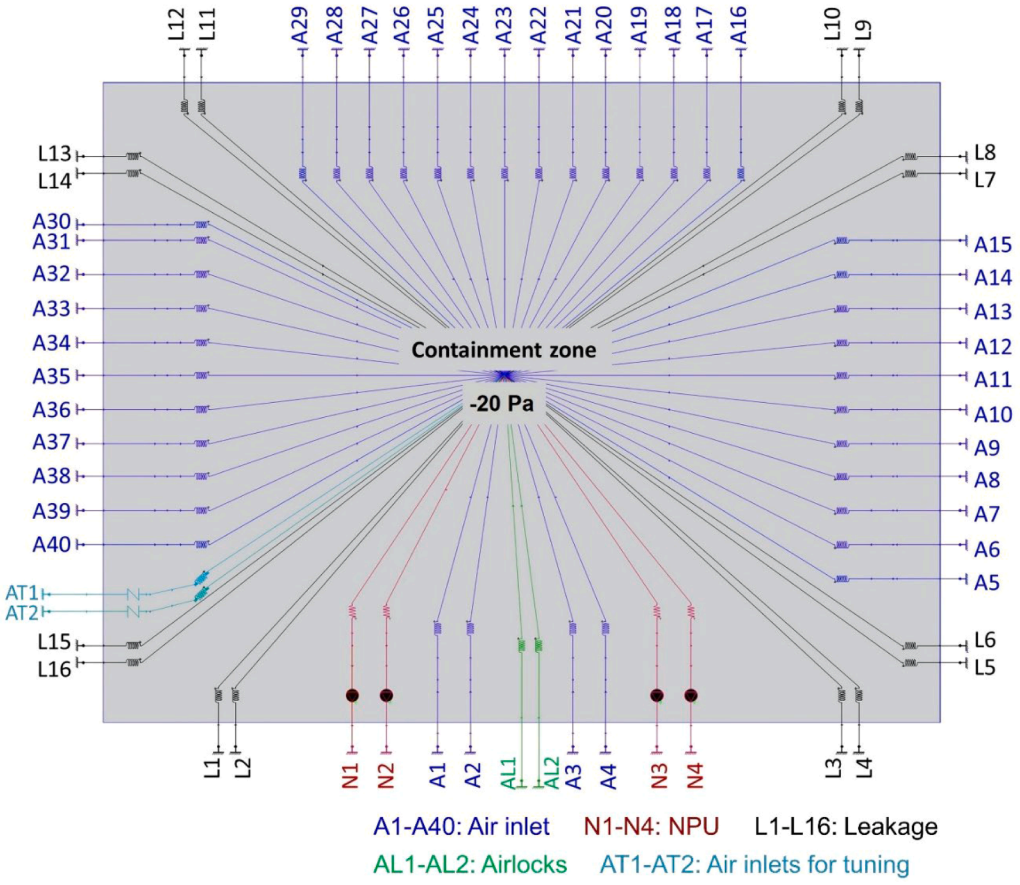

Fig. 6. Schematic of containment volume and mechanical ventilation system replicated in the network model.

entire tested duration (180 s) is displayed for visual clarity. The time series of p_i from a single internal reference sensor (B_{in}) on the internal wall of facade 2–3 (see Fig. 5) together with the associated instrumental uncertainty of ±2 Pa is also shown in the figure. The average p_i obtained from all internal pressure samples is also plotted in Fig. 7. It can be observed that the desired depressurization target of -20 Pa is approximately achieved on average. Additionally, the p_i remains negative for the entire duration displayed in the figure and across all internal measurement locations. The majority of instantaneous p_i captured by all other internal pressure sensors falls within the instrumental uncertainty bound of B_{in}. However, two internal pressure sensors located in close proximity to the fan (facade 0–1, Fig. 5) show that 3–5% of the samples lay outside the uncertainty bound. For all other sensors this is within a margin of 0.7%. Note that similar results are observed for *Scenario 2* (Section 3.2) with mechanical ventilation ON and wind ON (tested under different wind velocities and directions), although these results are not shown here for sake of brevity. This implies that p_i can be assumed to be spatially and temporally uniform within the containment zone, therefore, an individual sensor (B_{in}) can be considered as a representative sensor for analyzing p_i within the containment zone. Hence, for all further analysis of p_i, the results from sensor B_{in} are chosen to represent p_i measured within the containment volume.

3.2. Scenario 2: mechanical ventilation ON–wind ON

The external atmospheric wind conditions are generated as described in Section 2.1. WT tests are performed to investigate the influence of wind speed and direction on p_i. Three reference wind speeds (U_{ref} = 4.4, 6.5, 8.5 m/s) are used and each U_{ref} is tested for eight different wind directions (θ = 0–315° in steps of 45°). The boxplots of Fig. 8(a-c) show the temporal distribution of p_i obtained at the internal sensor B_{in} (see Section 3.1) for the corresponding reference wind velocities. The distribution of p_i corresponding to "no-wind" scenario is also added for comparison. The rectangular box at the center of each boxplot illustrates the interquartile range, which represents the range between the first quartile and the third quartile of the time series data. Thus, the length of the box corresponds to the spread of the middle 50% of the data. The median dividing the data into two halves is indicated by the red horizontal line positioned within the box. Vertical whisker lines (in blue) extend above and below the box to display the data range, excluding outliers. The lower whisker represents the first quartile of data, while the upper whisker represents the fourth quartile. Any values outside of the whiskers are considered outliers and are presented as individual data points in green. Therefore, the range of p_i (i.e., the minimum and the maximum values) is also evident in the boxplots.

In general, Fig. 8(a-c) indicates that p_i is influenced by the wind speed and direction. The median as well as the envelope of p_i (i.e., the length of the box as well as the whiskers) are found to increase in magnitude with increasing U_{ref}. Although the maxima remain around -20 Pa, irrespective of wind direction or speed, the minima tend to be lower (i.e., more negative) at higher wind speeds. Additionally, there is a concentration of outliers at the lower end of the boxplots. This may indicate occurrences of peak external suction pressures inducing negative peaks within the containment. Nevertheless, p_i is maintained negative under all wind speeds considered. Furthermore, when compared to "no-wind" scenario, the external wind effects tend to make the p_i in general more negative. This is attributed to the building geometry that results in higher overall external suction pressures compared to the overall external positive pressure on the building envelop as shown later in Figs. 10b and 10d. This is also illustrated in Fig. 8(d-f), which presents the boxplot of p_e from all external pressure sensors across various wind speeds and directions. The increase in the magnitude of p_e with rising wind speed is clearly visible. The black horizontal line marks 0 Pa. For most wind directions, majority of the measured p_e values indicate suction. Since the building model has ventilation inlet openings on all facades (although not uniformly distributed), the wind effects generate an effective negative p_i, as also found by Stathopoulos and Kozutsky [59].

A breach in containment is likely to occur at the locations where the magnitude of p_e is lower than p_i, namely when Δp is positive (as per Eq. 2). Therefore, although the absolute p_i is observed to be consistently negative, a breach is possible at specific locations. As an example, Fig. 9 (a-c) shows the Δp distribution at two ventilation component locations (*A3* on facade 0–1 – a positive external pressure zone, and *A38* on facade 3–0 – a negative external pressure zone) in form of a boxplot for θ = 0° and 45° for the three U_{ref} tested. The ventilation component located at the windward facade 0–1 (*A3*) shows no breach in containment, irrespective of the wind speed and direction, except for the two outliers for θ = 0° at the highest U_{ref} (Fig. 9c). However, for the ventilation component *A38* located on facade 3–0, containment breaches are observed for both

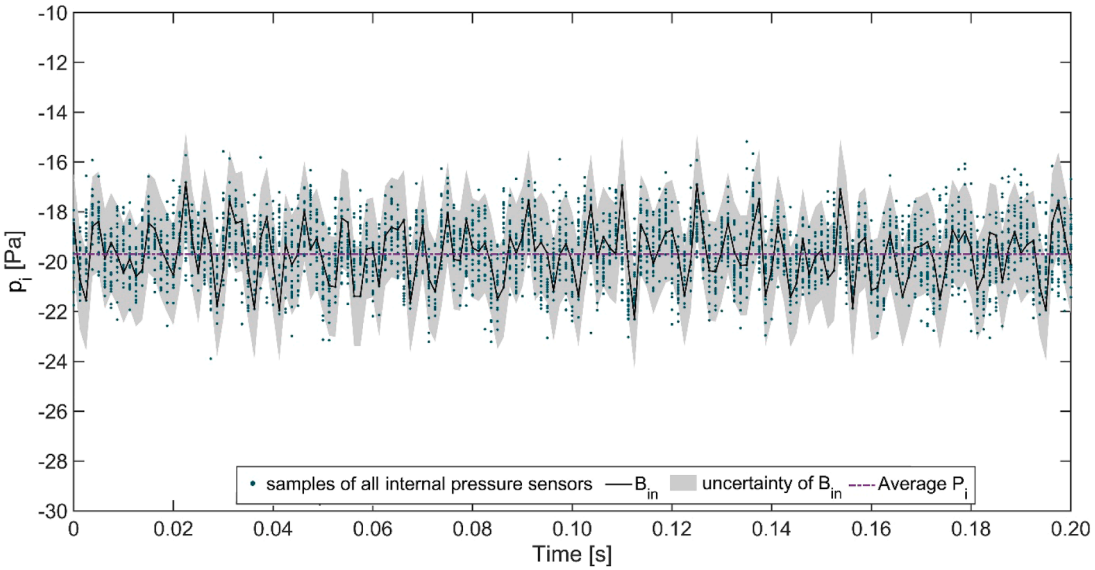

Fig. 7. Internal pressure time series within containment zone obtained from all 26 internal pressure sensors for the scenario: mechanical ventilation ON and wind OFF. Time series of reference sensor B_{in} with the associated instrumental uncertainty is also shown. To enhance visualization, a representative segment of 0.2 s from the entire tested duration (180 s) is displayed. The average P_i, derived from all internal pressure samples, is also included for reference.

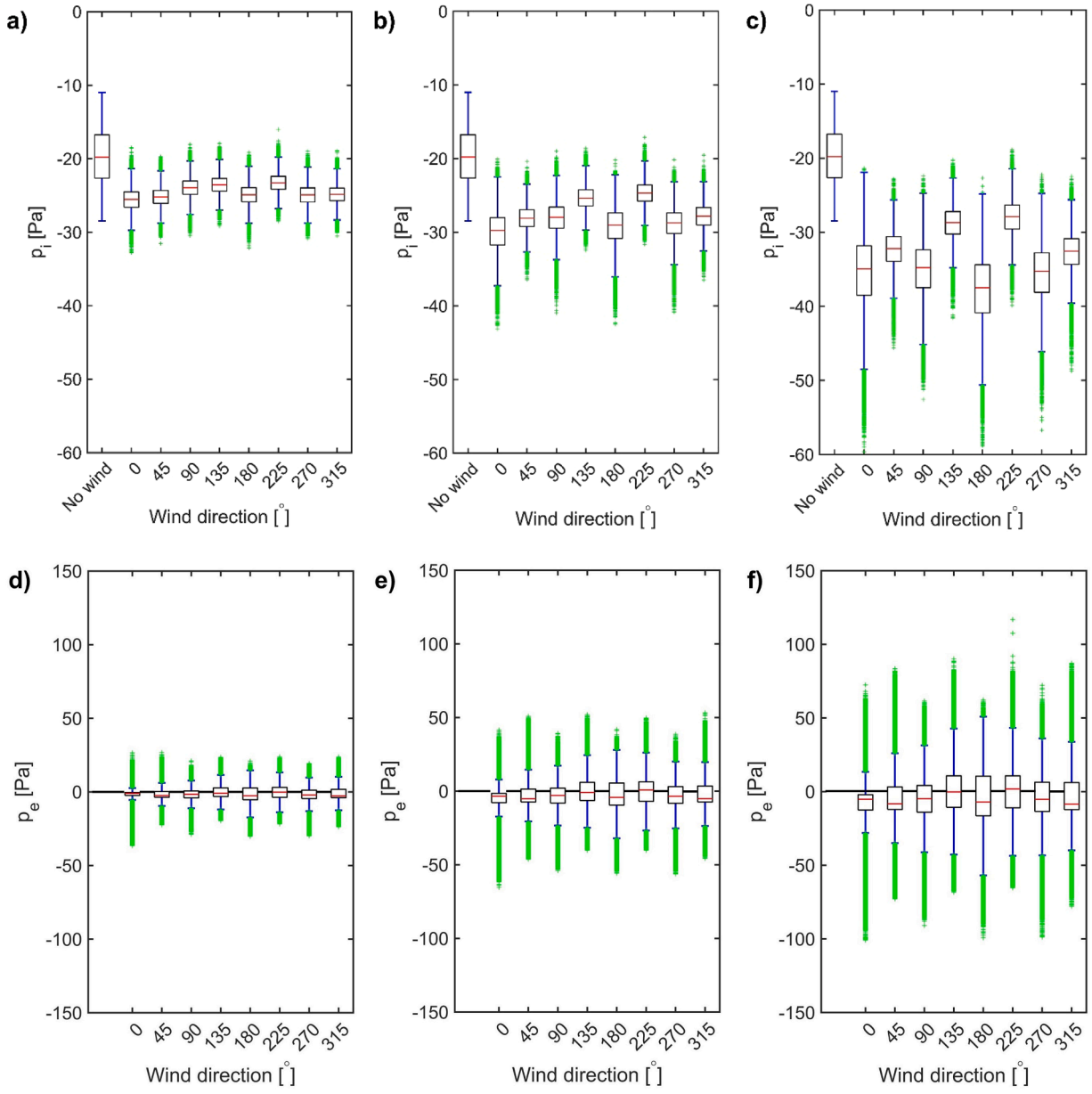

Fig. 8. Temporal distribution of p_i for eight wind directions (i.e., $\theta = 0^\circ$ - 315°) and three reference wind speeds (a) $U_{ref} = 4.4$, (b) 6.5, (c) 8.5 m/s. The scenario without wind is also shown for reference. Temporal distribution of p_e from all external pressure sensors for eight wind directions (i.e., $\theta = 0^\circ$ - 315°) and three reference wind speeds (d) $U_{ref} = 4.4$, (e) 6.5, (f) 8.5 m/s.

wind directions at the highest reference velocity $U_{ref} = 8.5$ m/s (see Fig. 9c). For $\theta = 0^\circ$, more than 25% of the time a breach is recorded, and for $\theta = 45^\circ$ there are occurrences of outliers exhibiting a breach. For $U_{ref} = 6.5$ m/s and 4.4 m/s, similar observations are made for $\theta = 0^\circ$, but with comparatively fewer occurrences of the breach (less than 25% for $U_{ref} = 6.5$ m/s and only several outliers for $U_{ref} = 4.4$ m/s). No occurrences of breach are detected at *A38* for the two lower reference velocities at $\theta = 45^\circ$.

The probability of containment breach is determined for all ventilation component locations exposed to wind (NPUs and air inlets) as well as leakages by calculating the ratio between the duration of recorded breaches and the overall measurement duration and is expressed in percentage terms. Fig. 10(a,c) shows the spatial distribution as well as the probability of containment breach expressed in percentage at each ventilation component for $\theta = 0^\circ$ and $\theta = 45^\circ$, respectively, and for $U_{ref} = 8.5$ m/s. The probability of the containment breach can reach up to 63% for $\theta = 0^\circ$ and 14% for $\theta = 45^\circ$. In order to better understand how the localized external pressure influences the probability of breach occurrence, the mean external pressure coefficient (C_{pe}) is shown in Fig. 10(b,d) for $\theta = 0^\circ$ and 45°. From these figures, the following pattern of C_{pe} is observed. For $\theta = 0^\circ$, on the windward facade 0–1 positive pressures are found, whereas negative pressures are prevalent on all other facades. This is due to the flow separation at the windward edges, causing high suction on the sidewalls (facades 1–2 and 3–0). The rear/leeward facade 2–3 is also dominated by negative pressures, though these pressures are lower in absolute value compared to those at the sidewalls. For $\theta = 45^\circ$, the windward facades (0–1 and 1–2) show positive pressures, whereas the leeward facades (2–3 and 3–0) depict negative pressures as a result of flow separation. Note that the asymmetry in the results arises from the asymmetrical positioning of the ventilation components as shown in Fig. 5. The C_{pe} distribution on the building facades indicates that:

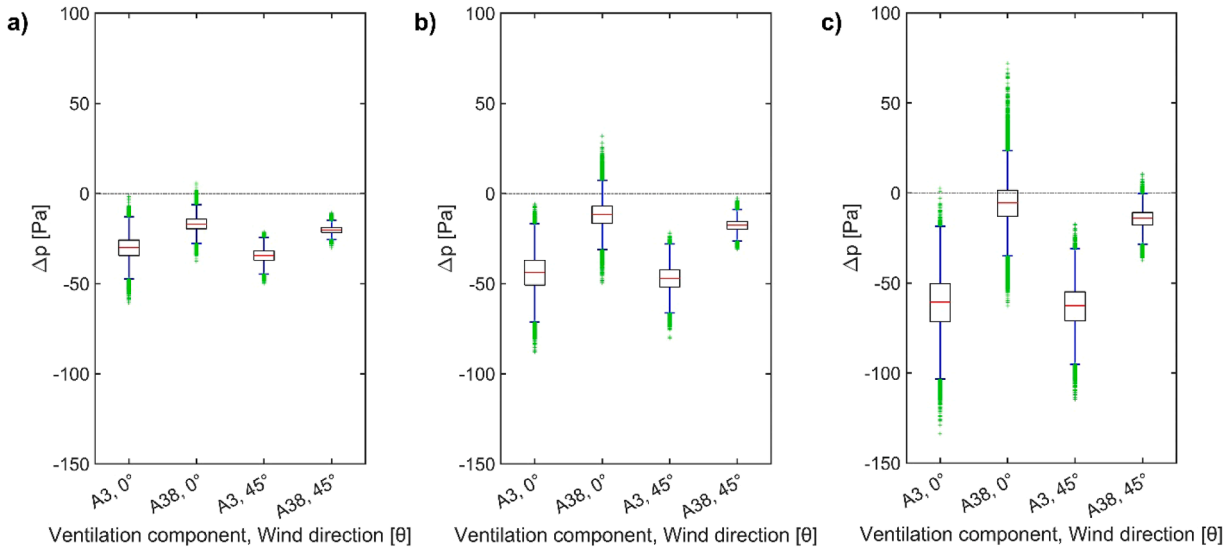

Fig. 9. Temporal ΔP distribution at two ventilation components (*A3* and *A38*) and two wind directions ($\theta = 0°$ and 45°) for (a) $U_{ref} = 4.4$, (b) 6.5 (c) 8.5 m/s.

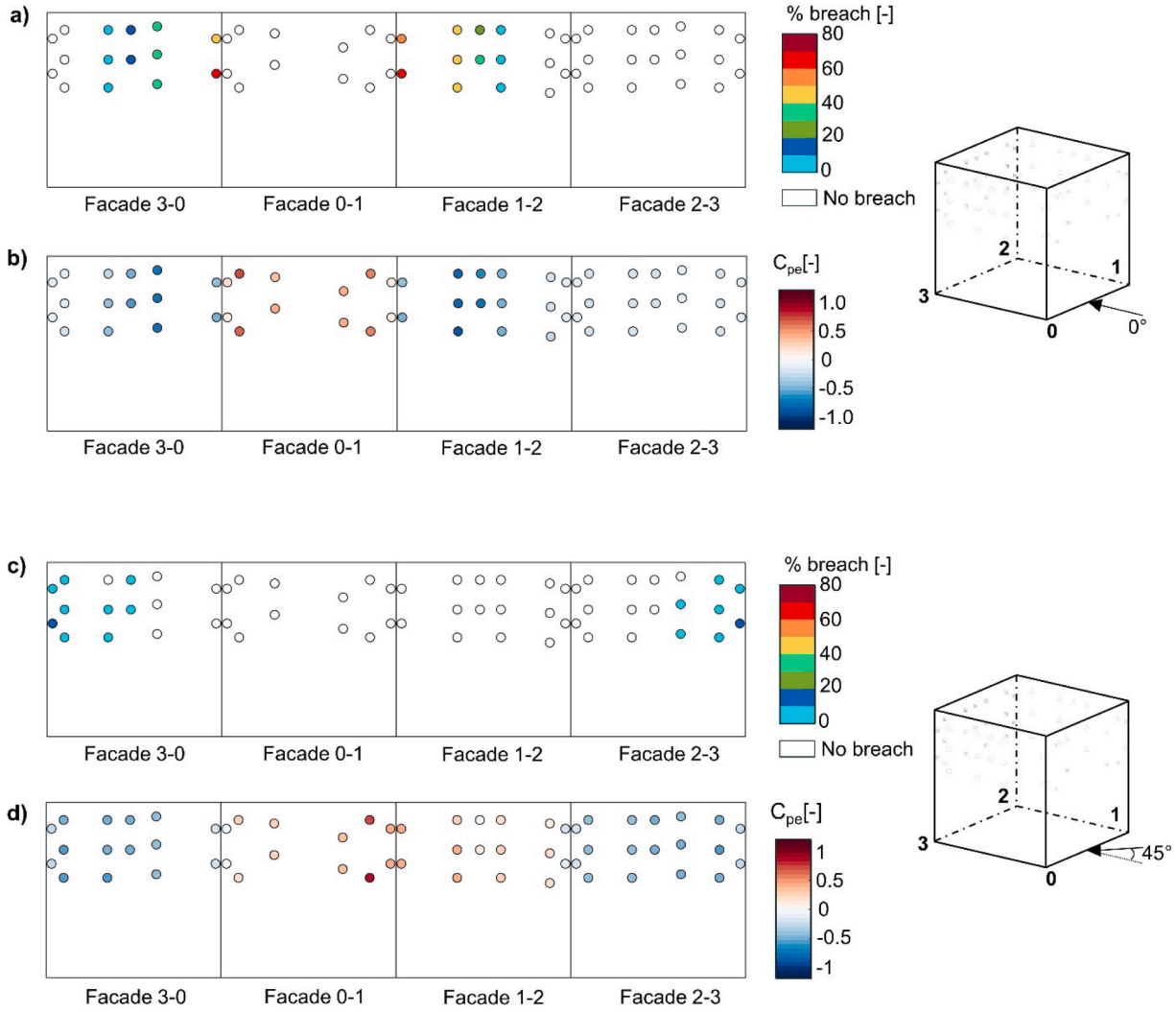

Fig. 10. Spatial distribution of containment breach likelihood for (a) $\theta = 0°$ and (c) 45° for $U_{ref} = 8.5$ m/s. Spatial distribution of temporally averaged external pressure coefficients (C_{pe}) for (b) $\theta = 0°$ and (d) 45°.

- For $\theta = 0°$ (Fig. 10a), the breach occurs where flow separation appear (facades 3–0 and 1–2), resulting in external suction pressures and negative C_{pe} values (Fig. 10b). The magnitude of the breach percentage increases towards the windward edge.
- For $\theta = 45°$ (Fig. 10c), the breach occurs along the leeward facades (3–0 and 2–3) where regions of negative C_{pe} are present (Fig. 10d).
- Similar results are also observed for $\theta = 90°$, 135°, 180°, 225°, 270°, and 315°, but are not shown for brevity.

Therefore, it can be concluded that while a negative p_i is consistently maintained, there is still the possibility of breaches in the containment zone due to high suction pressures on the building facades caused by external wind effects. The breach can occur in localized regions that depend on the building geometry and wind direction.

Fig. 11(a,b) shows the influence of wind speed on the probability of a containment breach. In particular, the figure depicts the percentage of containment breaches at pressure locations where breaches are recorded (see Fig. 10), for the three U_{ref} and for $\theta = 0°$ and 45°. The risk of breach evidently increases with the increasing of U_{ref}. Higher wind speeds induce larger suction pressures on the building facades, increasing the likelihood of these pressures to exceed the magnitude of internal depressurization. This observation is consistent for all wind directions investigated. For $\theta = 0°$ with $U_{ref} = 8.5$ m/s and 6.5 m/s, 30 and 21 pressure locations recorded breaches, respectively. Whereas for $U_{ref} = 4.4$ m/s only five locations experienced breach with a likelihood of occurrence of less than 0.5%. For $\theta = 45°$, a breach occurred at 16 pressure locations for $U_{ref} = 8.5$ m/s, while only four locations experiencing a breach for $U_{ref} = 6.5$ m/s and 4.4 m/s with breach percentage of less than 2.5%. Therefore, it can be inferred that the established -20 Pa of internal depressurization is not adequate to completely prevent containment breaches at any of the wind speeds investigated in this study. For higher wind speeds, the depressurization appears to be increasingly inadequate to prevent containment breaches.

3.3. Validation of the ventilation network model

The WT time series of p_e at the locations of all ventilation components exposed to wind is input in the network model to predict p_i within the containment volume. The calculation is performed for $U_{ref} = 8.5$ m/s with $\theta = 0°$ and $\theta = 45°$. Fig. 12(a,b) shows the p_i time series obtained from the WT tests (at sensor B_{in}, see Section 3.1) and the p_i predicted with the network model for $\theta = 0°$ and $\theta = 45°$, respectively. Fig. 12c compares the p_i predicted by the network model and measured in the WT. In general, the results of Fig. 12 exhibit a satisfactory qualitative agreement in terms of p_i between WT and the network model. However, discrepancies in the p_i fluctuations predicted by the network model are observed, particularly for $\theta = 45°$. Table 3 shows the deviations between WT and the network model calculated on p_i values at all instances. Almost 95% of instantaneous p_i values predicted by the network model fall within a deviation of 10% threshold tolerance from WT results, while more than 99.95% of the network model samples falls within a deviation of 20% threshold tolerance.

Table 4 presents a comprehensive comparison between the WT and the network model in terms of internal pressure statistics: $P_{i,mean}$ (mean), $P_{i,rms}$ (root-mean-square), $P_{i,\max}$ (maximum), and $P_{i,\min}$ (minimum) values, and percentage deviation. Notably, the statistics of internal pressure are also showing a strong consistency between the WT and the network model with all the parameters falling within a 5% deviation for $\theta = 0°$ and $\theta = 45°$.

The duration of a containment breach is also an important parameter, because the higher the duration of the breach, the higher the chances of suspended asbestos fibers escaping to the outdoor environment. Fig. 13 compares the duration of a breach predicted by the network model with the results from the WT tests, expressed as a percentage of the total measurement/simulation duration for all ventilation component locations. In general, a good agreement between the two datasets is observed. The highest absolute discrepancy in breach prediction occurs for $\theta = 0°$ with a deviation of 6%, while for $\theta = 45°$ the deviation decreases to 1%. In addition, it is important to note that the network model consistently underpredicts the duration of containment breach for $\theta = 0°$. This could be due to the discrepancy in the prediction of p_i fluctuations by the network model, as previously highlighted.

Overall, the network model exhibits a good performance in predicting the p_i distribution within the containment zones. However, slight discrepancies arise particularly in the prediction of p_i fluctuations which are more pronounced for $\theta = 45°$ (Fig. 12b). These discrepancies affect the determination of the containment breach occurrences and their duration. Several factors contribute to these discrepancies. First, the uncertainties inherent in the WT tests may affect the results, such as the ±2 Pa accuracy of the pressure measurement device. Additionally, it is not possible to achieve complete airtightness in the containment volume due to the openings around pressure tubes and electrical wires. This could introduce unintended leakages that can impact on the flow rate and measured pressure differences. This is evident in the higher magnitude of p_i fluctuations observed in the WT results compared to the network model predictions. Lastly, the behavior of the fan used in the WT tests, including rotational fluctuations, cannot be accurately replicated in the network model.

4. Practical implications

This section discusses the relevance of the present findings with respect to real application in asbestos removal worksites. From Section 3.2, it is observed that although a negative internal pressure is maintained throughout the measurement duration, localized containment breaches may occur (Figs. 8 and 10). In real asbestos abatement worksites, only internal pressures are monitored to assure that depressurization is maintained. However, this study demonstrates that the external-internal pressure difference (Δp) is actually the more suitable parameter to ensure the avoidance of instantaneous containment

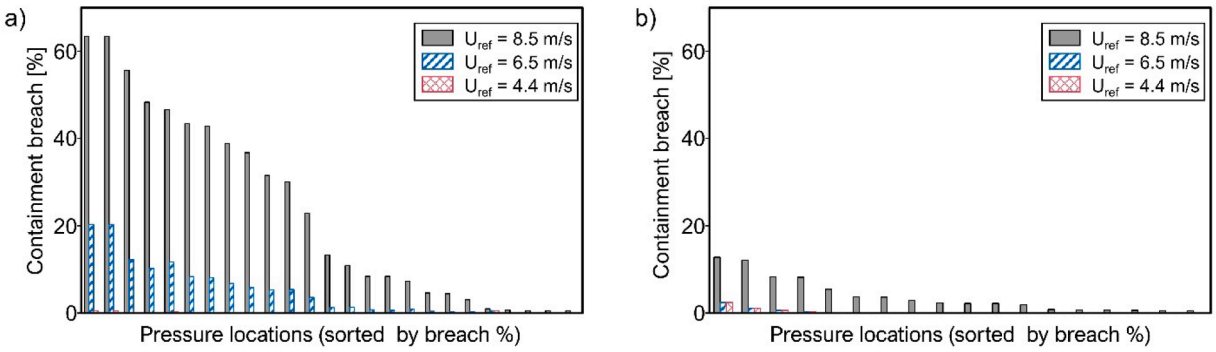

Fig. 11. Percentage containment breach at pressure sensor locations for the three U_{ref} at (a) $\theta = 0°$ and (b) $\theta = 45°$.

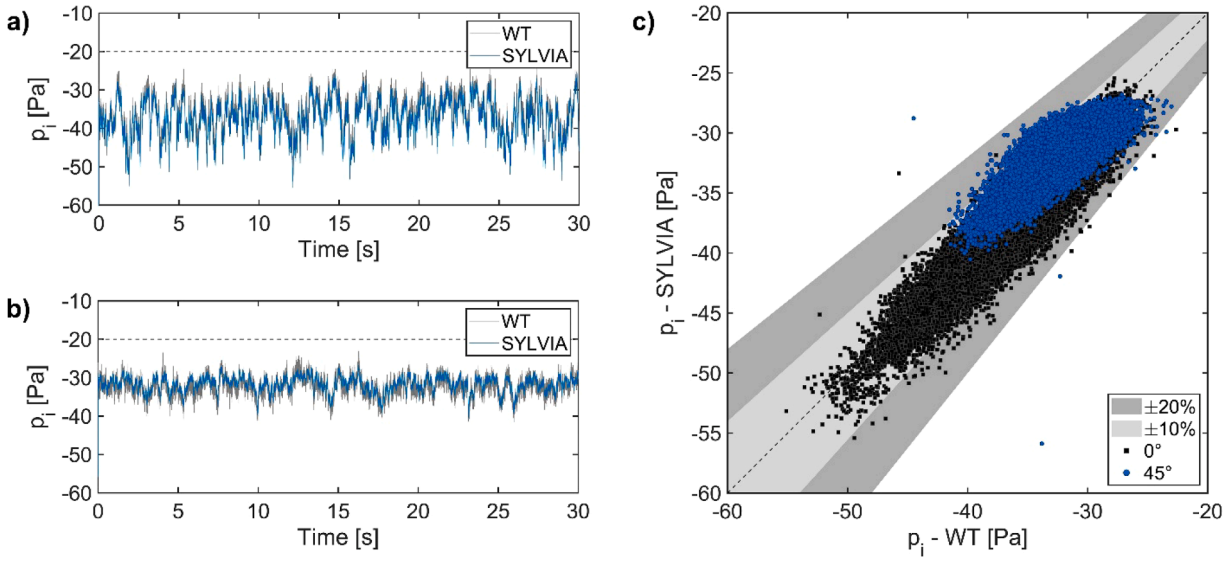

Fig. 12. Time-series of instantaneous internal pressures (P_i) obtained from WT tests and network model simulations for (a) $\theta = 0°$, (b) $\theta = 45°$ and (c) comparison between WT and network model.

Table 3
Comparison of p_i values obtained from WT tests and predicted by SYLVIA.

direction / tolerance	10%	20%
$\theta = 0°$	94.51%	99.95%
$\theta = 45°$	93.48%	99.96%

breaches under atmospheric winds.

The regions of flow separation, which can exhibit large external suction pressures, are susceptible to containment breach (Fig. 10). This implies that if there are any leakages or unintended openings in such regions, the chances of asbestos fibers escaping to the outdoor environment might be high. During the asbestos abatement process, it is advised to identify such regions with respect to the expected wind directions and to ensure a proper sealing of the containment zone.

Higher wind speeds are associated with an increased likelihood of breaches. Therefore, it is advised to conduct asbestos abatement activities on days characterized by low wind speeds whenever possible. This approach would minimize or entirely prevent the occurrence of containment breaches. Alternatively, in situations where high wind speeds are present, it is crucial to establish a higher internal depressurization to effectively avoid breaches.

The validated network model is a reliable tool for evaluating the probability of a containment breach, given the availability of external wind pressure data. The p_e data are required at all places of exposure to the external atmosphere, specifically at the locations of the ventilation components. The p_e data can be obtained from full-scale on-site pressure measurements, reduced-scale WT tests or validated CFD simulations. By incorporating the designed ventilation system into the network model and providing the p_e wind conditions, various scenarios can be simulated to evaluate the possibility of a containment breach.

The study highlighted that a depressurization value of -20 Pa is insufficient under all wind conditions and that the depressurization requirement to ensure containment is highly dependent on external wind conditions. As noted, most national guidelines recommend a single depressurization value, typically less than -20 Pa, regardless of wind conditions. Examples include Australia (-12 Pa) [60], Canada (-5 Pa) [61], Finland (-5 Pa, and -10 Pa for crocidolite) [62], France (-10 Pa) [16], Germany (-20 Pa) [63], the Netherlands (-20 Pa) [17], the United Kingdom (-5 Pa) [13] and the USA (-5 Pa) [19]. This discrepancy necessitates revisions to the recommended depressurization requirements, including detailed commentary on varying wind conditions to ensure practitioners are adequately informed about potential containment breaches. Further studies are needed to establish a relationship between depressurization requirements and likely wind conditions, enabling the development of clear and practical guidelines specific to different wind scenarios.

5. Summary and conclusions

Asbestos abatement processes from building interiors are recommended to be performed under controlled conditions, establishing an internal pressure that is lower than the pressure of the outdoor environment. The purpose is to prevent the release of airborne asbestos fibers into the surrounding atmosphere. However, atmospheric wind conditions can disrupt the controlled depressurization, potentially leading to temporary and local breaches. Therefore, it is essential to investigate and quantify the effects of wind speed and direction on internal depressurization. This research study presents ABLWT tests aimed at investigating the wind effects on an idealized building ($18 \times 18 \times 18$ m^3, at full-scale) equipped with a mechanically depressurized pollutant containment zone. Two scenarios with and without external wind conditions are analyzed, under three reference wind speeds ($U_{ref} = 4.4, 6.5,$

Table 4
Comparison of internal pressure statistics ($P_{i,mean}$, $P_{i,rms}$, $P_{i,\max}$, and $P_{i,\min}$) between WT tests and network model for $\theta = 0°$ and $\theta = 45°$.

	$\theta = 0°$			$\theta = 45°$		
	WT [Pa]	SYLVIA [Pa]	deviation [%]	WT [Pa]	SYLVIA [Pa]	deviation [%]
$P_{i,mean}$	-36.2	-37.4	-3	-32.4	-31.8	2
$P_{i,rms}$	36.5	37.7	-3	32.6	31.0	5
$P_{i,\max}$	-27.9	-28.5	-2	-27.7	-28.5	-3
$P_{i,\min}$	-46.6	-48.0	-3	-37.7	-36.6	3

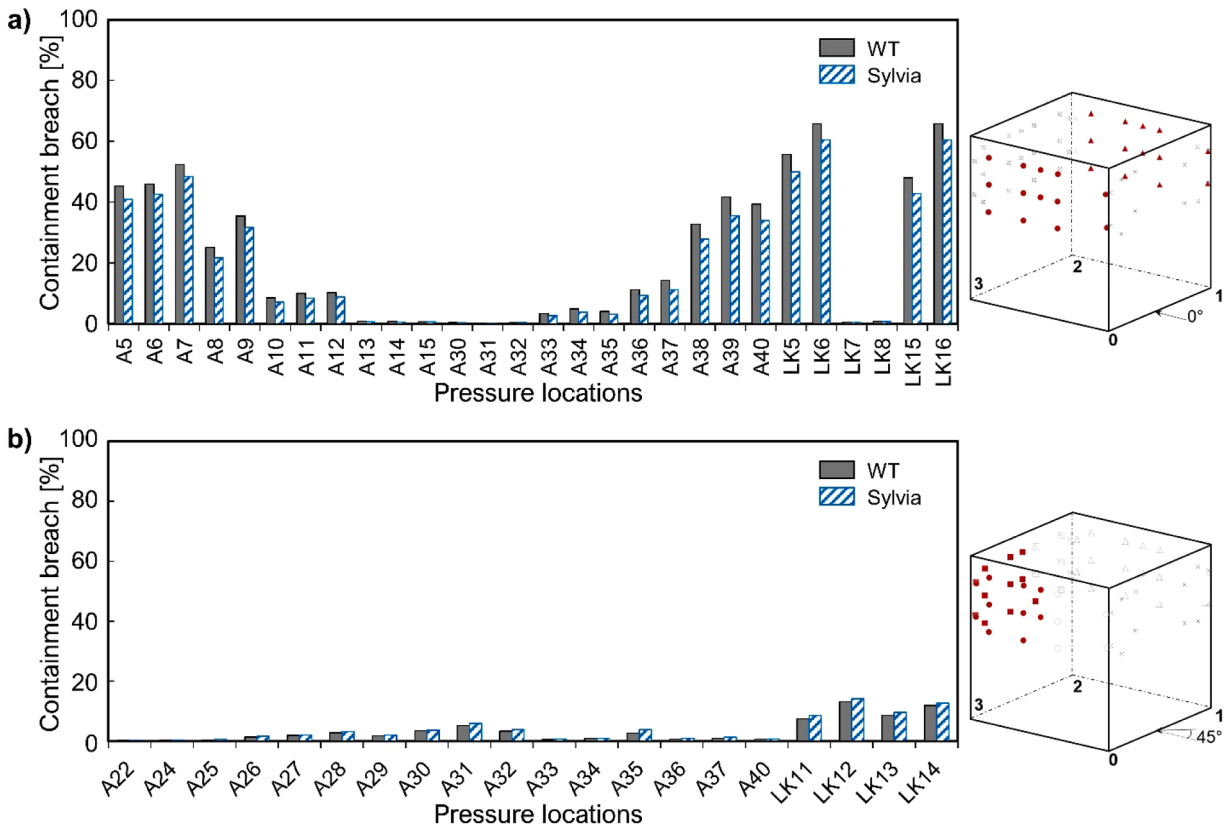

Fig. 13. Comparison of percentage containment breach duration predicted by the network model and determined from the internal-external pressure differences in the WT tests for (a) $\theta = 0°$ and (b) $\theta = 45°$. The isometric views of the building show the corresponding locations of containment breaches marked in red.

8.5 m/s) and eight wind directions (θ = 0–315° in steps of 45°). Furthermore, the implications of these findings for real asbestos abatement worksites are thoroughly discussed. However, it worth noting that this study also has the following limitations:

- The analysis focused on an isolated building with a simplified geometry, which represents only one of the endless real-world scenarios. However, the methodology can be adopted for more complex scenarios worldwide including the effects of surrounding buildings.
- The ventilation components are simplified and represented as ducts. For example, the backflow check valve for the air inlets are not explicitly modeled. However, the components are designed such that the aeraulic properties (i.e., the flow rate, pressure loss and aeraulic resistance) are well replicated.
- The pollutant particles (asbestos in this case) are not explicitly modeled for the experiment, rather assumed to be passive scalar considering the fact that the size of the asbestos particles that is hazardous ranges 3–5 μm in diameter. Physically modelling the particles poses significant challenges, as replicating the exact particle distribution characteristics may not be feasible. Moreover, such an approach could lead to highly specific scenarios, which might limit the generalizability of conclusions regarding the effects of wind on depressurization effectiveness.

Nevertheless, the following conclusions can be drawn from the study:

- The internal pressure distribution is found to be almost uniform spatially and temporally throughout the containment zone.
- A negative internal pressure is consistently maintained for all tested wind speeds and directions. However, the breach in containment occurs at localized regions where the external wind pressure is lower than the internal pressure.
- Containment breaches are identified in regions of flow separation, characterized by pronounced negative external wind pressure.
- The probability of a containment breach rises with higher wind speeds and varies depending on wind direction.

Then, the results from the WT tests are used to validate the ventilation network model SYLVIA. This validated model can be further utilized to investigate wind effects by:

- Altering design depressurization values to assess the adequacy of internal depressurization magnitudes.
- Testing a range of wind velocities to evaluate the existing depressurization requirements.
- Analyzing the effectiveness of the ventilation system in maintaining the depressurization with respect to:
  - the location of ventilation components relative to the prevailing wind direction;
  - the location of ventilation components relative to the building geometry;
  - the geometrical and aeraulic characteristics of the components of the ventilation system.

As a future research direction, the experimental methodology and the coupled WT – ventilation network model can be expanded to include more complex and realistic buildings. Incorporating surrounding structures into the study could provide deeper insights into the wind effects on asbestos abatement in built environments. Additionally, exploring the use of CFD simulations as an alternative to WT measurements for providing external wind pressures as SYLVIA inputs could enable analysis of a wider range of configurations. Moreover, this methodology can be applied to other fields where maintaining a pressure difference between the external and internal environments is essential, such as

hazardous pollutant treatment plants, lead removal worksites, overpressurized cabins of mobile machines or tractors used in solid waste landfills and hazardous waste sites.

CRediT authorship contribution statement

A.K.R. Jayakumari: Writing – original draft, Visualization, Formal analysis, Data curation. **R. Guichard:** Writing – review & editing, Supervision, Methodology, Investigation, Funding acquisition, Conceptualization. **S. Gillmeier:** Writing – review & editing, Supervision, Methodology, Investigation, Conceptualization. **A. Ricci:** Writing – review & editing, Supervision, Methodology, Investigation, Conceptualization. **B. Blocken:** Writing – review & editing, Supervision, Methodology, Investigation, Funding acquisition, Conceptualization.

Declaration of competing interest

The authors declare the following financial interests/personal relationships which may be considered as potential competing interests:

One of the co-authors, Bert Blocken, serves as an Editor for this journal. One of the co-authors, Alessio Ricci, serves as an Assistant Editor for this journal. If there are other authors, they declare that they have no known competing financial interests or personal relationships that could have appeared to influence the work reported in this paper.

Acknowledgments

The project is undertaken in collaboration with the Institut National de Recherche et de Sécurité (INRS), France, and its support throughout this project is greatly appreciated.

Data availability

Data will be made available on request.

References

[1] J.A. Malik, S. Marathe, Ecological and Health Effects of Building Materials, Springer International Publishing, Cham, 2022. ISBN 978-3-030-76073-1.
[2] W.R. Barclay, Asbestos: An Industrial Asset with a Health Cost, J. Am. Med. Assoc. 252 (1984) 96.
[3] G.R. Wagner, R.A. Lemen, Asbestos. International Encyclopedia of Public Health, Elsevier, 2017, pp. 176–182.
[4] R.F. Dodson, S.P. Hammar, Asbestos: Risk Assessment, Epidemiology, and Health Effects, CRC Press, Florida, USA, 2005.
[5] N. Alpert, M.V. Gerwen, E. Taioli, Epidemiology of mesothelioma in the 21st century in Europe and the United States, 40 years after restricted/banned asbestos use, Transl. Lung Cancer Res. 9 (2020) S28–S38.
[6] European Economic, Social Committee, Working With Asbestos in Energy Renovation (own-initiative opinion) (CCMI/166-EESC-2018-01-01), 2019.
[7] L.P. Thives, E. Ghisi, J.J. Thives Júnior, A.S. Vieira, Is asbestos still a problem in the world? A current review, J. Environ. Manage 319 (2022) 115716.
[8] D.L. Keyes, B.P. Price, J. Chesson, Guidance for controlling asbestos-containing materials in buildings: 1985 edition, United States (1985). PB-86-116522/XAB, TRN: 86-004424.
[9] S. Young, L. Balluz, J. Malilay, Natural and technologic hazardous material releases during and after natural disasters: a review, Sci. Total Environ. 322 (2004) 3–20.
[10] R.J. Lee, D.R. Van Orden, Airborne asbestos in buildings, Regulat. Toxicol. Pharmacol. 50 (2008) 218–225.
[11] G. Kakoulaki, C. Maduta, G. Tsionis, P. Zangheri, M. Bavetta, Identification of Vulnerable EU Regions Considering Asbestos Presence and Seismic Risk, Publications Office of the European Union, Luxembourg, 2023. ISBN 978-92-68-04254-0.
[12] W.C. D'Angelo, R.C. Spicer, M.J. Mease, Asbestos Removal in Occupied Buildings: Sophisticated Procedures For Structures with Operating HVAC Systems. First edition, 1987. New Jersey, ISBN 0-917097-08-4.
[13] Great Britain Health and Safety Executive (HSE), Asbestos: The licensed Contractors guide. First edition, 2006. ISBN 978 0 7176 2874 2.
[14] F. Dubernet, R. Guichard, A. Romero-Hariot, Amiante. Aéraulique des Chantiers Sous confinement, Guide Pratique De ventilation. First edition, 2018. ISBN 978-2-7389-2385-1.
[15] World Health Organization Regional Office for Europe, National Programmes for Elimination of Asbestos-related Diseases: Review and Assessment, WHO Regional Office for Europe, Copenhagen, 2012.
[16] Legifrance, Arrêté Du 8 Avril 2013 Relatif Aux Règles techniques, Aux Mesures De Prévention Et Aux Moyens De Protection Collective à Mettre En Oeuvre Par Les Entreprises Lors D'opérations Comportant Un Risque D'exposition à L'amiante, 2013. URL, https://www.legifrance.gouv.fr/loda/id/JORFTEXT000027324535/. accessed: 09-10-2021.
[17] Ministerie van Sociale Zaken en Werkgelegenheid, Artikel 43 (Asbestverwijdering, Punt 3) Van Bijlage XIIIa (Werkveldspecifiek Certificatieschema Voor De Procescertificaten Asbestinventarisatie En Asbestverwijdering, 2016.
[18] Service public fédéral (SPF) Emploi, Travail et Concertation Sociale, Code du bien-être au travail. Livre VI: Agents chimiques, cancérigènes, Mutagènes Et reprotoxiques, Titre 3, Amiante, 2017.
[19] Occupational Safety and Health Administration (OSHA), Asbestos, Code of Federal Regulations, 29 CFR 1910.1001 and 29 CFR 1926.58, 2019.
[20] D. Pocock, S. Bennett, J. Saunders, Ventilation of Enclosures For Removal of Asbestos Containing materials. Research Report RR988. Health and Safety Laboratory For the Health and Safety Executive, 2013, pp. 1–45.
[21] I. Kulmala, M. Linnainmaa, A. Kokkonen, K. Heinonen, T. Kanerva, A. Säämänen, Performance of Asbestos Enclosure Ventilation: Laboratory Evaluation of Complex Configuration, Ann. Work Expo Health 65 (2021) 1085–1095.
[22] A. Papadopoulos, R. Guichard, T. Van Hoof, J.R. Fontaine, B. Blocken, Measurements of wind effects on the efficacy of asbestos containment in a high-rise building, in: Proceedings of Roomvent & Ventilation Conference, Helsinki, Finland, 2-5 June 2018, 2018.
[23] I.P. Castro, A.G. Robins, The flow around a surface-mounted cube in uniform and turbulent streams, J. Fluid. Mech. 79 (1977) 307–335.
[24] T. Stathopoulos, Design and fabrication of a wind tunnel for building aerodynamics, J. Wind Eng. Indust. Aerody. 16 (1984) 361–376.
[25] J.E. Cermak, Wind-tunnel development and trends in applications to civil engineering, J. Wind Eng. Indust. Aerody. 91 (2003) 355–370.
[26] J.D. Holmes, Wind Loading of Structures. Third edition, Taylor & Francis, 2004. ISBN 0-203-30164-1.
[27] A.M. Aly, Atmospheric boundary-layer simulation for the built environment: Past, present and future, Build. Environ. 75 (2014) 206–221.
[28] B. Blocken, T. Stathopoulos, J.P.A.J. van Beeck, Pedestrian-level wind conditions around buildings: Review of wind-tunnel and CFD techniques and their accuracy for wind comfort assessment, Build. Environ. 100 (2016) 50–81.
[29] S. Kato, S. Murakami, A. Mochida, S. Akabayashi, Y. Tominaga, Velocity-pressure field of cross ventilation with open windows analyzed by wind tunnel and numerical simulation, J. Wind Eng. Indust. Aerody. 44 (1992) 2575–2586.
[30] Etheridge, Unsteady flow effects due to fluctuating wind pressures in natural ventilation design - Instantaneous flow rates, Build. Environ. 35 (2000) 321–337.
[31] Q. Chen, Ventilation performance prediction for buildings: A method overview and recent applications, Build. Environ. 44 (2009) 848–858.
[32] B. Wang, D.W. Etheridge, M. Ohba, Wind tunnel investigation of natural ventilation through multiple stacks. Part 2: Instantaneous values, Build. Environ. 46 (2011) 1393–1402.
[33] P. Karava, T. Stathopoulos, A.K. Athienitis, Airflow assessment in cross-ventilated buildings with operable façade elements, Build. Environ. 46 (2011) 266–279.
[34] D. Etheridge, A perspective on fifty years of natural ventilation research, Build. Environ. 91 (2015) 51–60.
[35] Y. Tominaga, B. Blocken, Wind tunnel experiments on cross-ventilation flow of a generic building with contaminant dispersion in unsheltered and sheltered conditions, Build. Environ. 92 (2015) 452–461.
[36] D. Golubić, W. Meile, G. Brenn, H. Kozmar, Wind-tunnel analysis of natural ventilation in a generic building in sheltered and unsheltered conditions: Impact of Reynolds number and wind direction, J. Wind Eng. Indust. Aerody. 207 (2020) 104388.
[37] D.P. Albuquerque, P.D. O'Sullivan, G.C. Da Graça, Effect of window geometry on wind driven single sided ventilation through one opening, Energy Build. 245 (2021) 111060.
[38] Y. Tominaga, B. Blocken, Wind tunnel analysis of flow and dispersion in cross-ventilated isolated buildings: impact of opening positions, J. Wind Eng. Indust. Aerody. 155 (2016) 74–88.
[39] N. Le Roux, X. Faure, C. Inard, S. Soares, L. Ricciardi, Reduced-scale study of wind influence on mean airflows inside buildings equipped with ventilation systems, Build. Environ. 58 (2012) 231–244.
[40] N. Le Roux, X. Faure, C. Inard, S. Soares, L. Ricciardi, Reduced-scale study of transient flows inside mechanically ventilated buildings subjected to wind and internal overpressure effects, Build. Environ. 62 (2013) 18–32.
[41] T. Le Dez, J. Richard, C. Inard, N. Le Roux, F. Demouge, X. Faure, L. Ricciardi, Reduced-scale study of the coupling between thermal and wind effects on the ventilation systems of nuclear facilities, Int. J. Ventil. 20 (2021) 1–19.
[42] Y. Lee, T.H. Liang, H. Tanaka, Non-linearity of Pressure Differentials Induced By Wind and Mechanical Ventilation, 15, 1983, pp. 47–58.
[43] A.K.R. Jayakumari, R. Guichard, A. Ricci, S. Gillmeier, B. Blocken, Towards an improved wind effect assessment for asbestos abatement: A methodology for reduced-scale experiments, J. Environ. Manage 370 (2024) 122698.
[44] Institut de Radioprotection et de Sûreté Nucléaire (IRSN), Physical Modelling of the SYLVIA V11 software. Institut de Radioprotection et De Sûreté Nucléaire, Paris, France, 2022.
[45] H.P.A.H. Irwin, The design of spires for wind simulation, J. Wind Eng. Indust. Aerody. 7 (1981) 361–366.
[46] A.K.R. Jayakumari, S. Gillmeier, A. Ricci, B. Blocken, R. Guichard, Scaling effects on experimentally obtained pressures on an idealized building: Possible implications towards asbestos containment, J. Wind Eng. Indust. Aerody. 239 (2023) 105442.

[47] B. Blocken, P. Moonen, T. Stathopoulos, J. Carmeliet, A numerical study on the existence of the Venturi-effect in passages between perpendicular buildings, J. Eng. Mech. - ASCE 134 (12) (2008) 1021–1028.
[48] B. Blocken, T. Stathopoulos, J. Carmeliet, Wind environmental conditions in passages between two long narrow perpendicular buildings, J. Aerospace Eng. - ASCE 21 (4) (2008) 280–287.
[49] Turbulent Flow Instrumentation Pty Ltd, Getting Started: Series 100 Cobra Probe (v3.7), 2015.
[50] VDI-3783, Verein Deutscher Ingenieure.Environmental Meteorology - Physical Modeling of Flow and Dispersion Processes in the Atmospheric Boundary Layer Application of Wind Tunnels, 2000.
[51] E. Simiu, R.H. Scanlan, Wind Effects on Structures: an Introduction to Wind Engineering, Second ed, John Wiley & Sons, Inc, 1986. ISBN 047186613X.
[52] D. Etheridge, M. Sandberg, Building ventilation: Theory and measurement. First edition, John Wiley & sons, UK, 1996. ISBN 047196087X.
[53] ASHRAE, ASHRAE Handbook: Fundamentals (SI Ed), American Society of Heating, Refrigerating and Air-Conditioning Engineers, Inc, 2001, p. 26, 1–26.32.
[54] J.H. Oh, G.A. Kopp, D.R. Inculet, The UWO contribution to the NIST aerodynamic database for wind loads on low buildings: Part 3. Internal pressures, J. Wind Eng. Indust. Aerody. 95 (2007) 755–779.
[55] ScanivalveCorp, MPS4264 Miniature pressure Scanner Hardware and Software manual, Software version 2.07, Scanivalve Corp, WA, USA, 2019.
[56] H.P.A.H. Irwin, K.R. Cooper, R. Girard, Correction of distortion effects caused by tubing systems in measurements of fluctuating pressures, J. Wind Eng. Indust. Aerod. 5 (1979) 93–107, 93–107.
[57] J. Axley, Multizone Airflow Modeling in Buildings: History and Theory, HVAC&R. Res. 13 (2007) 907–928.
[58] U.M. Asher, L.R. Petzold, Computer Methods for Ordinary Differential Equations and Differential-Algebraic Equations. First edition, SIAM, Philadelphia, USA, 1998.
[59] T. Stathopoulos, R. Kozutsky, Wind-induced internal pressures in buildings, J. Struct. Eng. 112 (1986) 2012–2026.
[60] Safe work Australia, How to Safely Remove Asbestos Code of Practice, 2011. ISBN 978-0-642-33317-9.
[61] M. Ziembicki, E., A. Karpinski, Technical Guideline to Asbestos Exposure Management Programs, 2018. ISBN: 978-0-660-24459-4.
[62] Ministry of Social Affairs and Health, Government Degree on the Safety of Asbestos Work, 798, 2015. Helsinki, Finland.
[63] Bundesanstalt für Arbeitsschutz und Arbeitsmedizin (BAuA), Technische Regel für Gefahrstoffe. (TRGS) 519 Asbest: Abbruch-, Sanierungs- oder Instandhaltungsarbeiten, 2014, pp. 1–65.